Available online at www.sciencedirect.com
ScienceDirect
Magnetic Resonance Imaging 26 (2008) 513 – 522
MAGNETIC RESONANCE IMAGING

SNR and functional sensitivity of BOLD and perfusion-based fMRI using arterial spin labeling with spiral SENSE at 3 T☆

Joanna E. Perthen, Mark Bydder, Khaled Restom, Thomas T. Liu *

Center for Functional MRI and Department of Radiology, University of California, San Diego, La Jolla, CA 92093, USA

Received 5 June 2007; revised 4 September 2007; accepted 8 October 2007

Abstract

Blood oxygenation level-dependent (BOLD) functional magnetic resonance imaging (fMRI) studies using parallel imaging to reduce the readout window have reported a loss in temporal signal-to-noise ratio (SNR) that is less than would be expected given a purely thermal noise model. In this study, the impact of parallel imaging on the noise components and functional sensitivity of both BOLD and perfusion-based fMRI data was investigated. Dual-echo arterial spin labeling data were acquired on five subjects using sensitivity encoding (SENSE), at reduction factors (R) of 1, 2 and 3. Direct recording of cardiac and respiratory activity during data acquisition enabled the retrospective removal of physiological noise. The temporal SNR of the perfusion time series closely followed the thermal noise prediction of a $\sqrt{R}$ loss in SNR as the readout window was shortened, with temporal SNR values (relative to the R=1 data) of 0.72 and 0.56 for the R=2 and R=3 data, respectively, after accounting for physiological noise. However, the BOLD temporal SNR decreased more slowly than predicted even after accounting for physiological noise, with relative temporal SNR values of 0.80 and 0.63 for the R=2 and R=3 data, respectively. Spectral analysis revealed that the BOLD trends were dominated by low-frequency fluctuations, which were not dominant in the perfusion data due to signal processing differences. The functional sensitivity, assessed using mean F values over activated regions of interest (ROIs), followed the temporal SNR trends for the BOLD data. However, results for the perfusion data were more dependent on the threshold used for ROI selection, most likely due to the inherently low SNR of functional perfusion data.

Keywords: fMRI; Parallel imaging; SENSE; BOLD; Perfusion; SNR

1. Introduction

Parallel imaging techniques exploit the unique spatial sensitivities of individual coils within a receive array to construct a full field-of-view (FOV) image from data that is undersampled in k-space [1]. For blood oxygenation level dependent (BOLD) functional magnetic resonance imaging (fMRI) studies, parallel imaging methods have been used to decrease the readout times of single-shot echoplanar imaging (EPI) [2] and spiral acquisitions [3]. This reduction in the readout time was shown to increase the detection power of BOLD fMRI studies in brain regions where magnetic susceptibility inhomogeneities can lead to significant image distortions and signal loss when long readout windows are used. Parallel imaging has also been used to increase the spatial resolution of BOLD fMRI studies [4].

Perfusion-based fMRI with arterial spin labeling (ASL) is finding increasing use, in part because perfusion is a fundamental physiological quantity that may provide a more accurate reflection and localization of neural activity as compared to BOLD [5,6]. In addition, when used in combination with BOLD measures, the perfusion signal can be used to estimate functional changes in the cerebral metabolic rate of oxygen consumption [7]. In contrast to BOLD images, ASL images can be acquired with either short echo time (TE) gradient echo acquisitions or spin-echo acquisitions that significantly reduce susceptibility-related signal losses [8]. The use of parallel imaging in ASL studies can lead to further reductions in both susceptibility-related distortions and TE, as recently demonstrated in a resting-state ASL study [9].

☆ This work was funded in part by a grant from the National Institutes of Health (R01 NS051661).

* Corresponding author. Tel.: +1 858 822 0542; fax: +1 858 822 0605.
E-mail address: ttliu@ucsd.edu (T.T. Liu).

0730-725X/$ – see front matter © 2008 Elsevier Inc. All rights reserved.
doi:10.1016/j.mri.2007.10.008

The cost of parallel imaging is a decrease in the image signal-to-noise ratio (SNR) since fewer k-space samples are acquired per image. For a single image, image SNR decreases by $g\sqrt{R}$, where R is the reduction (or acceleration) factor by which the acquisition window is shortened, and g is a spatially variant noise amplification factor that is determined by the k-space sampling strategy and coil geometry [10]. However, it is temporal SNR rather than single image SNR that is of prime importance in fMRI studies. Recent studies have reported that the temporal SNR of BOLD [3,4,11] and resting perfusion [9] EPI image data decreases more slowly than the $\sqrt{R}$ prediction (which assumes that thermal noise dominates). Since temporal SNR depends not only on thermal noise but is also influenced by any processes leading to time course variations, such as physiological fluctuations and scanner instabilities, these studies concluded that changes in reduction factor altered the relative contributions of thermal and physiological noise components. For example, De Zwart et al. [11] showed that their BOLD data were consistent with a model in which the noise is expressed as the sum of a thermal noise component that increased with reduction factor and a physiological component that remained constant across reduction factors.

In order to further investigate the origins of the temporal SNR trends discussed above, BOLD and perfusion-based fMRI data were acquired at three different reduction factors (R=1, 2 and 3) using sensitivity encoding (SENSE) [10]. Cardiac and respiratory activity were recorded during data acquisition and used to retrospectively remove physiological noise from the data. This allowed a direct assessment of the effects of these noise sources on various measures of functional sensitivity and temporal SNR across reduction factors. In the interests of isolating the effects of the shortened readout on temporal SNR, temporal and spatial resolution as well as TE were kept constant across reduction factors, and experiments focused on a region of the brain (the visual cortex), which does not suffer from extreme geometric distortions.

2. Methods

2.1. Data acquisition

Five healthy adult subjects (three male; age range, 27–39 years) participated in the study after giving informed consent. All data were acquired on a GE Signa Excite 3-T whole-body system equipped with an eight-channel receive-only head coil (MRI Devices, Gainesville, FL, USA). A body coil was used for radiofrequency transmission.

High-resolution structural scans were acquired with a magnetization prepared 3D fast spoiled gradient echo sequence (TI 450 ms, TR 7.9 ms, TE 3.1 ms, flip angle 12°, FOV 250×250×160 mm, matrix 256×256×124).

Functional data were acquired using a PICORE QUIPSS II pulsed ASL sequence [12,13] with dual gradient echo spiral readout. Four 7-mm slices were positioned parallel to the calcarine sulcus, and imaging parameters were as follows: TR 2 s, TI1 600 ms, TI2 1500 ms, TE 9.1 and 30 ms, flip angle 90°, matrix 64×64, FOV 240 mm. Small bipolar gradients (b=2 s/mm^2) placed immediately before the first echo were used to reduce signal from large vessels. The visual stimulus consisted of a maximum contrast checkerboard flashing at 8 Hz, alternating with a blank screen (rest state) at the same mean luminance as the checkerboard. The stimulus was presented in a block design consisting of an initial 40-s rest period, followed by four cycles of 20-s flashing checkerboard/40-s rest. Each functional run lasted 4 min 40 s. Subjects were instructed to fixate on a small square in the center of the screen that was visible throughout each run.

For each subject, two functional runs were acquired at each reduction factor (1, 2 and 3) in randomized order. The readout window was 19.4 ms for R=1 (fully sampled k-space) and was shortened by reducing the sampling density in the radial direction to obtain reduction factors of 2 and 3 with readout windows of 9.7 and 6.5 ms, respectively. In order to create coil sensitivity profiles for image reconstruction, reference images in which k-space was fully sampled were acquired for each reduction factor, with the number of interleaves set to the reduction factor in each case so as to produce images with similar distortions.

Cardiac and respiratory effort data were continuously recorded throughout the scan session using a pulse oximeter (InVivo, Orlando, FL, USA) and a respiratory effort transducer (BIOPAC systems, Goleta, CA, USA). Scanner timing pulse data were also recorded to enable synchronization of the physiological data to the acquired images.

2.2. Data reconstruction

All data were reconstructed offline using the SENSE iterative gridding approach designed for arbitrary k-space trajectories [14], implemented in MATLAB (The Mathworks, Natick, MA, USA). A Kaiser–Bessel gridding kernel of width 5, oversampling factor 2 and shape α=2.34 was used [15], with 30 iterations. A small regularization term is typically employed in SENSE reconstruction to ensure safe convergence [16], but since the effect of regularization on SNR properties is not clear [17], the current study used only a minimal regularization term on the order of machine precision. Although the fully sampled k-space images (R=1) could be reconstructed using conventional methods, a SENSE reconstruction ensures SNR optimization and sensitivity correction and makes comparison between the three reduction factors more straightforward. Coil sensitivity maps were generated from the reference images.

2.3. Data analysis

The high-resolution anatomical data were segmented using the FSL FAST image segmentation tool [18]. Gray and white matter masks were created for each subject by

selecting voxels containing at least 70% gray or white matter, respectively. "Nonactivated" gray and white matter regions of interest (ROIs) were defined by manually delineating and excluding the visual cortex from the gray and white matter masks. All ASL images were motion-corrected by registration to the first fully sampled (R=1) dataset using AFNI software [19], and the first four data points were removed from each time course to allow for the approach to the steady state.

Estimates of image SNR were calculated using the approach described by Glover and Lai [20]. In short, a new image series was formed by extracting the control images from the ASL run. The even- and odd-numbered images from this series were then separately averaged, and the sum and difference of these average images was calculated. The image SNR was calculated as the mean value from the "nonactivated" ROI in the sum image divided by the standard deviation over the same region in the difference image. For each subject, the image SNR values were normalized by the value obtained for R=1. The differences between the normalized image SNR values (n=5) for the R=2 and R=3 data and the thermal noise predictions (0.71 and 0.58, respectively) were assessed using two-tailed t tests. For all statistical tests, $P<.05$ was taken to be significant.

Functional time series were calculated from the raw tag/control image series as follows: perfusion time series were created from a surround subtraction of the first echo data (TE=9.1 ms), using a filter of the form (−0.5, 1, −0.5) [21]. BOLD time courses were created from a surround average of the second echo data (TE=30 ms), using a filter of the form (0.5, 1, 0.5)/2. Additional *short-TE* BOLD time courses were created from a surround average of the first echo data in order to investigate the effect of TE on temporal SNR trends.

Temporal SNR values were calculated voxelwise for the perfusion, BOLD and short-TE BOLD time series, as the ratio of the mean signal to the temporal standard deviation, after removal of linear trends. These values were computed with and without the application of physiological noise reduction (see below for details of noise reduction). The SNR values were normalized to the R=1 values and then averaged over nonactivated gray and white matter ROIs to generate average values for each subject. The differences between the resulting normalized temporal SNR values (n=5) for the R=2 and R=3 cases and the thermal noise predictions (0.71 and 0.58, respectively) were assessed using two-tailed t tests. To assess the confounding effects of any remaining functional activation in the nonactive ROIs, a second set of temporal SNR values were calculated after first regressing out any stimulus-related components from the voxelwise data and then compared to thermal noise predictions.

To assess the impact of SENSE on the detection of functional activity, the functional perfusion and BOLD data were modeled using a general linear model which included regressors describing the stimulus function convolved with a hemodynamic response function (gamma density function), a constant term, a linear term and terms describing cardiac and respiratory fluctuations. Physiological noise terms were removed using a retrospective imaged based correction method previously described by Glover et al. [22] and adapted for use with arterial spin labeling data by Restom et al. [23]. In order to compare the effect of different acquisitions on the ability to detect functional activation, F statistics were calculated on a pixelwise basis both with and without the use of physiological noise reduction. Active ROIs were created for a range of F thresholds between 2 and 14 for the perfusion data and between 20 and 140 for the BOLD data (the higher thresholds used for the BOLD data reflect its higher intrinsic SNR). For each F threshold and each functional scan, voxels exceeding the threshold and having at least 1 neighboring voxel also above the threshold were defined as active. Then, for each subject, an ROI was defined as the union of the active voxels over the three reduction factors. ROIs were defined with and without the use of physiological noise reduction, and all ROIs had a contribution of at least six active voxels from each reduction factor. The mean F value for each reduction factor over each ROI was calculated and expressed as a fraction of the R=1 case. Differences between the mean F ratios for the three reduction factors were assessed for significance using paired t tests.

In order to investigate the frequency distribution of the energy in the noise for the three reduction factors, spectral analyses were performed on the perfusion and BOLD time series. Voxelwise power spectra were calculated after the removal of the mean signal and linear trends and were normalized to the area of the R=1 spectrum. For each subject, spectra were averaged over the nonactivated gray matter ROI and subsequently group averaged.

3. Results

3.1. Image SNR

Fig. 1 shows the normalized image SNR values for the raw (A) first and (B) second echo data. The image SNR values were not significantly ($P>.05$) different from the purely thermal noise prediction of a $\sqrt{R}$ reduction in SNR with reduced acquisition times, although the difference for the R=3 first echo data was nearly significant (P=.06) with the observed value being lower than the predicted value.

3.2. Temporal SNR

Representative temporal SNR maps from a single subject are shown in Fig. 2. For both perfusion and BOLD images, the temporal SNR visibly decreases as the reduction factor increases.

Fig. 3 shows the normalized temporal SNR values as a function of reduction factor for (A) gray matter perfusion data, (B) gray matter BOLD data, (C) white matter BOLD data, (D) gray matter short-TE BOLD data and (E) white

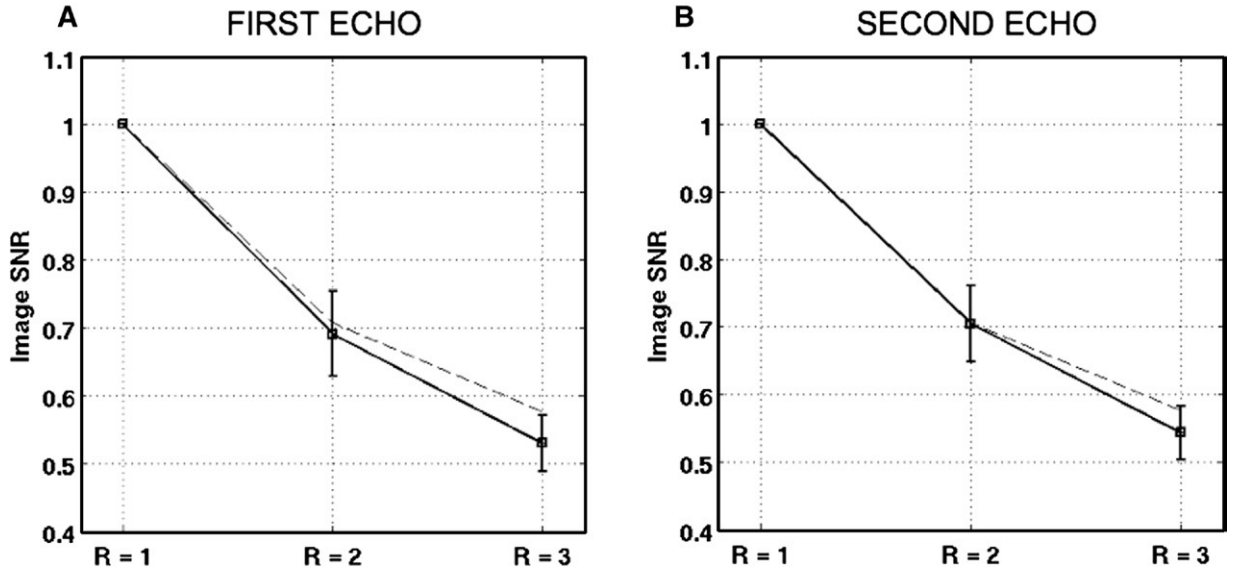

Fig. 1. Mean normalized image SNR values for the first (A) and second (B) echo data. Dotted lines show the predicted values assuming a purely thermal noise model ($1/\sqrt{R}$). Error bars show 1 standard deviation across subjects.

matter short-TE BOLD data, with (diamonds) and without (squares) the application of physiological noise reduction. White matter perfusion data are not reported since the sequence parameters were not optimized to acquire reliable white matter perfusion values. For the gray matter perfusion data, the normalized SNR values are not significantly different from the thermal noise model predictions (dotted lines), with the exception of the R=2 values without noise reduction, which exhibited significantly (P<.03) higher values than the theoretical prediction. The normalized temporal SNR values for the gray matter BOLD data (with and without physiological noise reduction) were significantly higher (P<.02) than the predicted values for both acceleration factors. In contrast, the short-TE gray matter

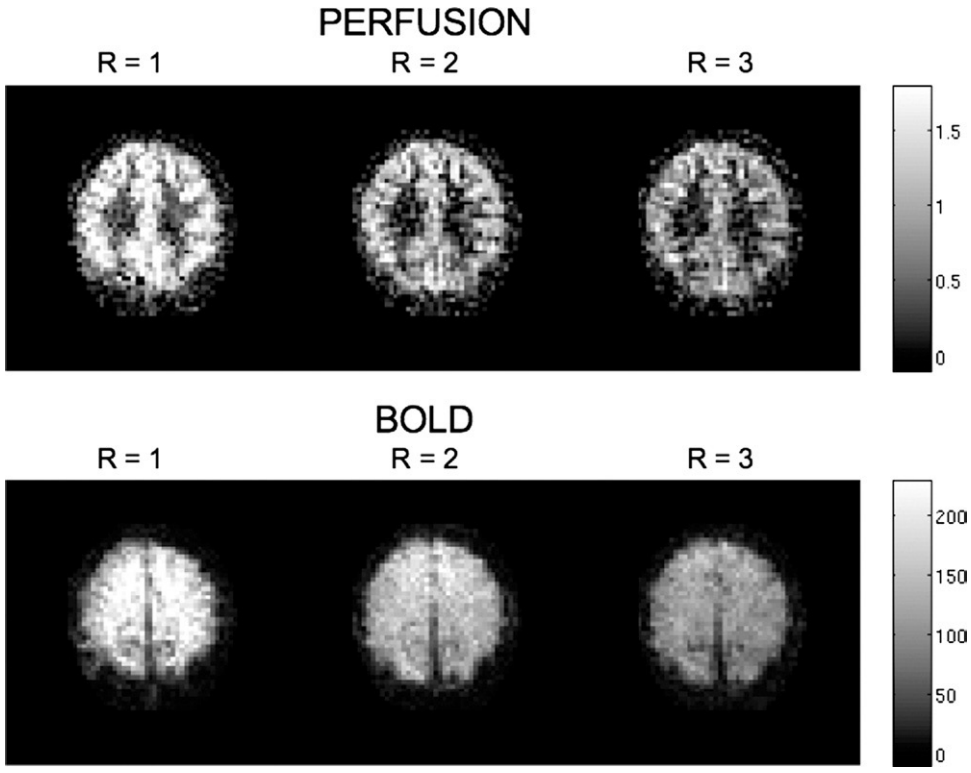

Fig. 2. Perfusion and BOLD temporal SNR maps from a representative subject. Data for each reduction factor from a single slice are shown.

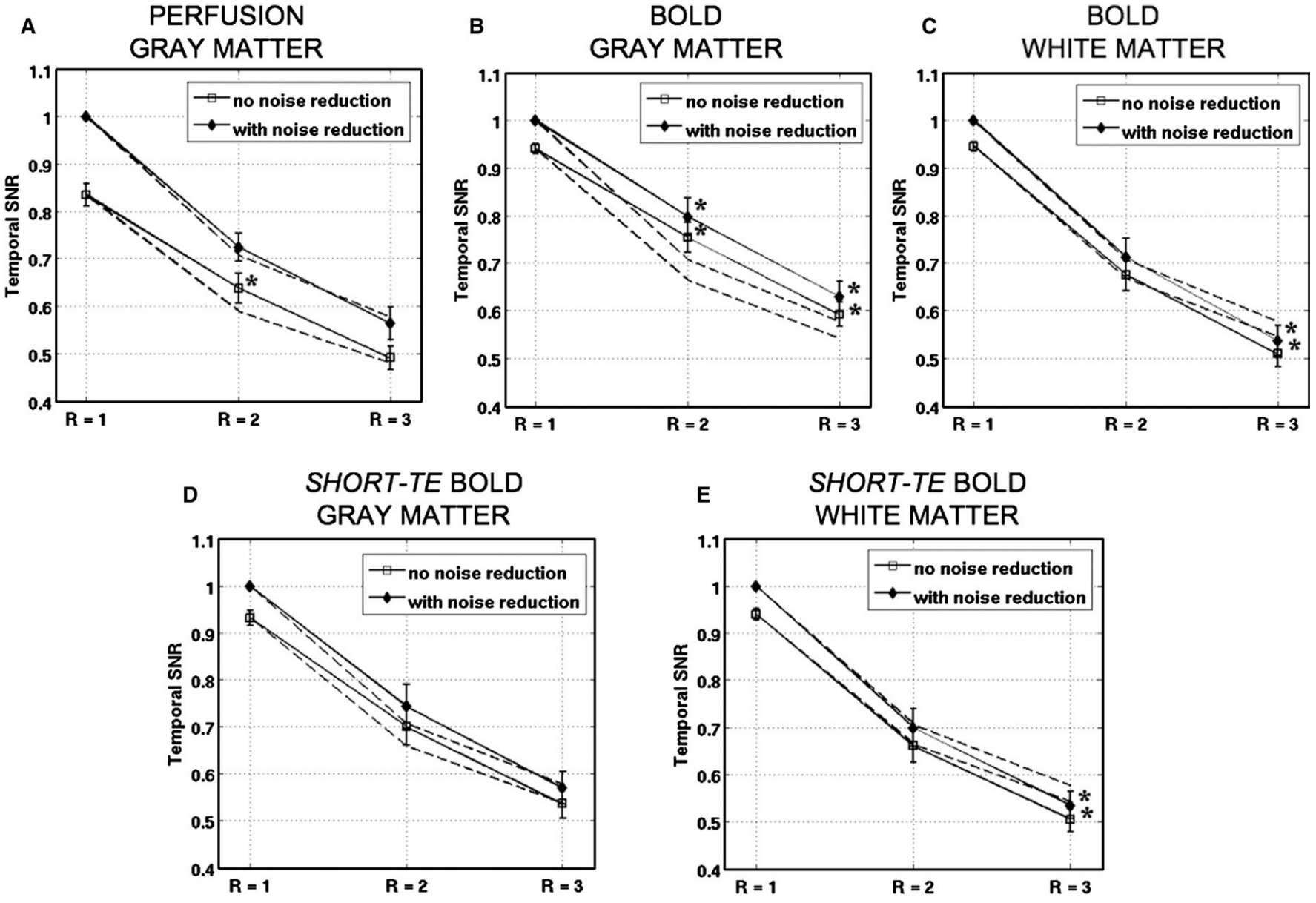

Fig. 3. Normalized temporal SNR values for gray matter perfusion (A), gray matter BOLD (B), white matter BOLD data (C), short-TE gray matter BOLD (D) and short-TE white matter BOLD (E). Values are shown with (diamond) and without (squares) physiological noise reduction. Error bars indicate one standard deviation over subjects. The dotted lines show the expected normalized temporal SNR given a $\sqrt{R}$ relationship (thermal noise only), relative to the R=1 data point. Significant differences from the thermal noise values are indicated by an asterisk (P<05).

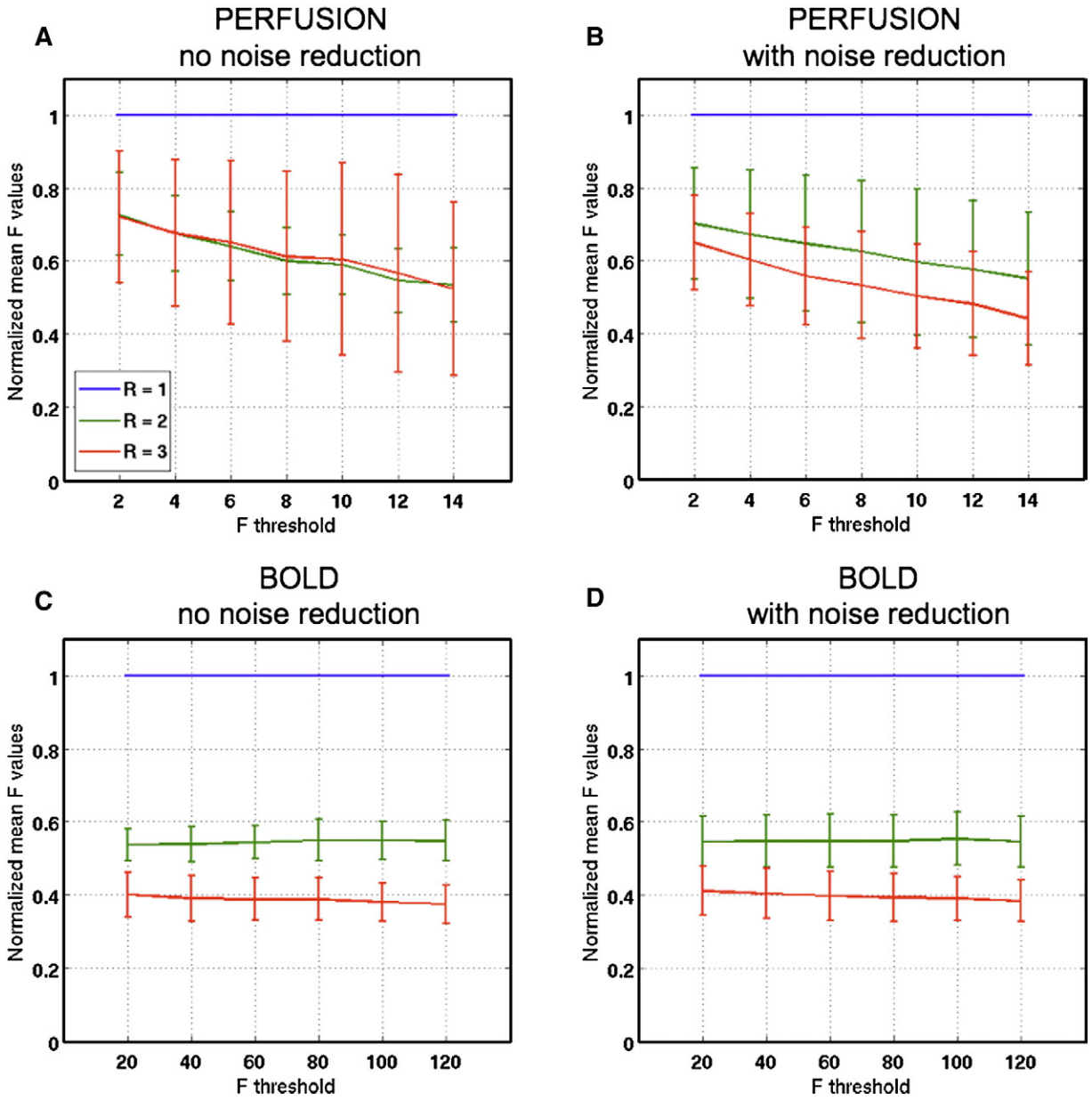

Fig. 4. Normalized mean F values within active ROIs as a function of *F* threshold for the perfusion data without (A) and with (B) noise reduction and the BOLD data without (C) and with (D) noise reduction. All values are expressed relative to the *R*=1 data, and the error bars show one standard deviation over subjects.

BOLD values were not significantly different from the theoretical prediction. For the white matter BOLD and short-TE BOLD values, the *R*=2 values were not significantly different than the predicted values, while the *R*=3 values were significantly lower ($P<.04$) than predicted. The data shown were obtained with the nonactivated ROI defined in the Methods section. Very similar trends were observed for the data after removal of stimulus-related components, with the exception of the perfusion *R*=2 values with noise reduction, which were slightly higher than the theoretical prediction ($P<.05$) when the stimulus-related components were removed.

3.3. Functional sensitivity

The mean *F* statistics, normalized to the *R*=1 data, are shown in Fig. 4 for the perfusion and BOLD data, analyzed both with and without physiological noise reduction. For the perfusion data, the mean *F* values show a dependence on the *F* threshold, with the mean *F* value for the undersampled data decreasing relative to the *R*=1 data as the *F* threshold increases. The best fit line for each data set has a slope that is significantly ($P<.01$) different from zero, with mean slopes [in units of (100*normalized *F* value)/(*F* threshold)] of −1.2±0.03 and −1.6±0.09 for the *R*=2 and *R*=3 cases,

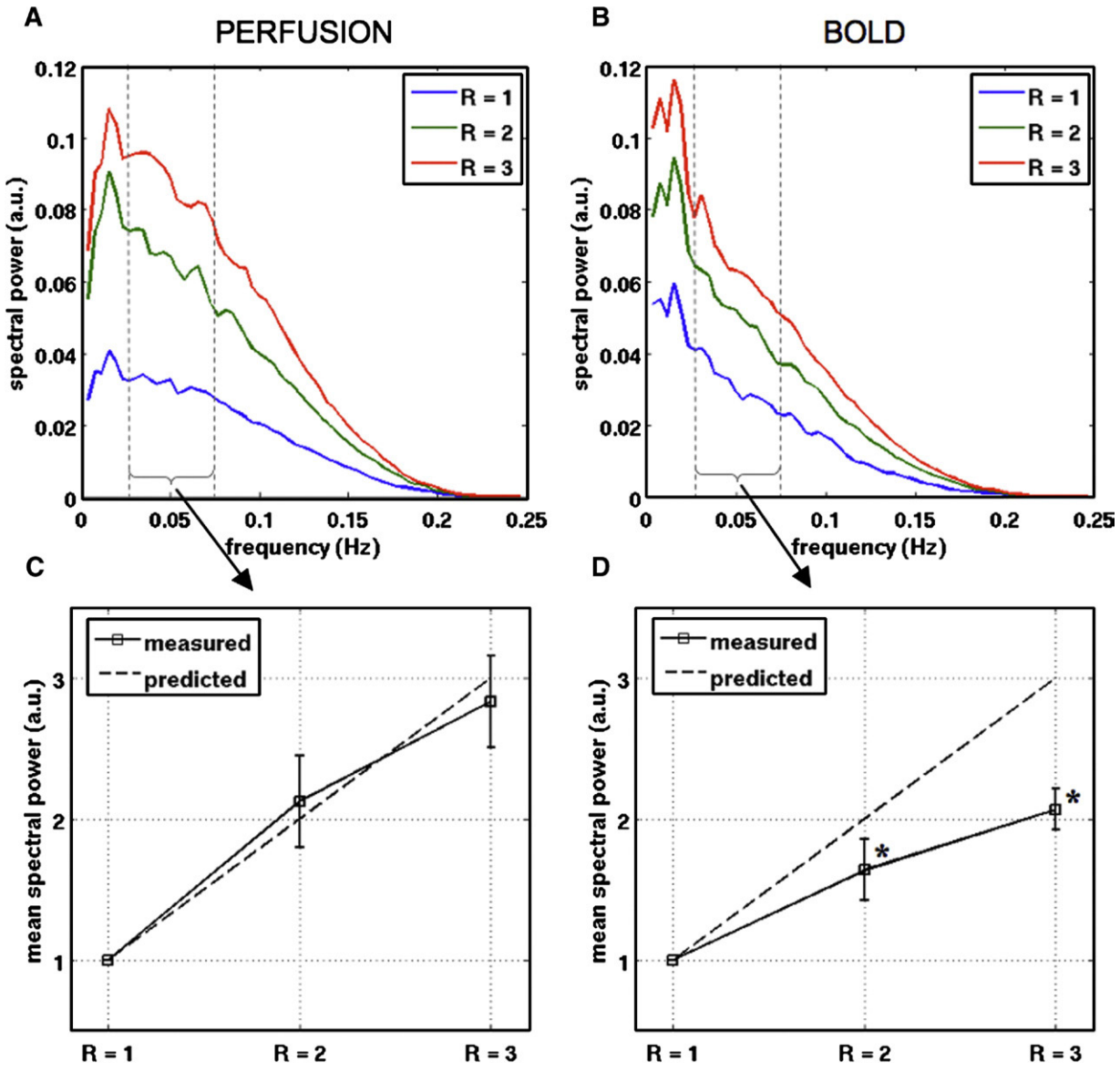

Fig. 5. Group-averaged power spectra for the perfusion time series (A) and BOLD time series (B). Spectra were averaged over the nonactive gray matter ROIs, after physiological noise reduction. The small peaks at ~0.016 Hz represent residual activation that remains after removal of the visual cortex voxels. The mean spectral power over the range 0.025–0.075 Hz for the perfusion and BOLD data are shown in (C) and (D), respectively, normalized to the R=1 data. Error bars indicate one standard deviation over subjects, and the dotted lines show the expected values given a thermal noise model. Significant differences from the model are indicated by an asterisk (P<.05).

respectively, with physiological noise reduction and corresponding values of −1.6±0.1 and −1.5±0.09 without noise reduction. Although the mean F for the undersampled data is significantly less than the R=1 case for all F thresholds, there is no significant difference between the R=2 and R=3 data at any F thresholds, with or without noise reduction.

In contrast, the BOLD data are relatively more stable over a wide range of F thresholds. Although the slopes of the best fit lines are significantly different to zero in all cases except that of R=2 with physiological noise reduction, the slopes are relatively small (0.003±0.003 and −0.03±0.002 for the R=2 and R=3 cases, respectively, with physiological noise reduction and 0.01±0.003 and −0.02±0.003 without noise reduction). The R=2 and R=3 data are significantly different from each other and from the R=1 data at all F thresholds (P<.004) both with and without noise reduction. The square root of the mean F statistics (used as a measure of SNR) for the R=2 and R=3 cases were not significantly different to the gray matter BOLD temporal SNR values reported in Fig. 3B.

3.4. Spectral analysis

Fig. 5 shows the power spectra for the (A) perfusion and (B) BOLD time series, calculated after physiological noise reduction within the nonactivated gray matter ROIs. Both the

perfusion and the BOLD spectra exhibit a zero at 0.25 Hz, reflecting the effects of the low pass filtering inherent in the surround subtraction and average procedures [21]. Small peaks are evident at ~0.016 Hz, representing residual functional activation that remains within the nonactive ROIs. Fig. 5C shows the mean power in the perfusion spectra over a frequency range (0.025–0.075 Hz; denoted by dashed vertical lines in panels A and B), chosen to exclude those frequencies affected by residual functional activation, as well as those dominated by filter effects. The thermal noise model predicts a linear relationship between spectral power and acceleration factor, and the calculated values are not significantly different from the predicted values (P=.3 for R=2 and P=.5 for R=3). In contrast, the power in the BOLD spectra (shown in Fig. 5D) increases much more slowly than the thermal noise prediction (P<.02 for both cases).

4. Discussion

The use of parallel imaging techniques allows the reduction of the readout window by a factor of R if spatial resolution is kept constant. In cases in which the dominant source of noise is thermal, we would expect to observe an SNR reduction of $g\sqrt{R}$, where g is the noise amplification factor. In this study, we have investigated the SNR characteristics and functional sensitivity of perfusion and BOLD fMRI data acquired with SENSE. The image SNR measured in the raw data (both first and second echoes) did not differ significantly from a $\sqrt{R}$ trend, consistent with recent work showing that the noise amplification factor is spatially homogeneous and close to unity for SENSE reconstruction with a spiral trajectory and an eight-channel wraparound head coil [24].

For the perfusion data, we found a decrease in temporal SNR with increasing acceleration factor (both prior to and after physiological noise reduction). Before the removal of cardiac and respiratory noise, the temporal SNR was significantly higher than the predicted value for the R=2 case, but not for the R=3 case. The greater-than-predicted temporal SNR for R=2 tends to indicate a decrease in the contribution of cardiac and respiratory noise as the readout window is shortened from R=1 to R=2, while the agreement with prediction at R=3 may reflect a balance between a reduction in physiological noise with shorter readout window and increased noise amplification at the higher reduction factor (consistent with the lower temporal SNR values observed in white matter at R=3 that are discussed below). After noise reduction, the observed SNR values were not significantly different from the predicted values, suggesting that thermal noise is the dominant noise source after removal of cardiac and respiratory signal components. In contrast, Wang et al. [9] found that the temporal SNR of their resting perfusion time series was slightly improved (R=2) or remained the same (R=3) with the use of parallel imaging. The discrepancy in results may be due to the use of shorter TEs as the acceleration factor was increased in reference [9]. The use of a shorter TE with higher acceleration factors can offset the expected temporal SNR reduction by increasing the perfusion time series signal (i.e., less signal decay) and decreasing physiological noise contributions [25]. In the present study, we avoided this confounding effect by using constant TE across acceleration factors.

In agreement with prior studies, the temporal SNR values of the gray matter BOLD time series prior to physiological noise reduction were found to be significantly greater than the predicted values [3,4,11]. In contrast to the results observed with the perfusion data, the gray matter temporal SNR values after physiological noise reduction remained significantly higher than the predicted values, suggesting the presence of additional noise components not accounted for by the respiratory and cardiac regressors. As shown in Fig. 5D, the power of low frequency signal components (below ~0.1 Hz) increases more slowly than predicted with acceleration factor, consistent with the higher than expected temporal SNR values at the higher acceleration factors.

Low-frequency fluctuations in the BOLD signal have been widely reported and are often referred to as 1/f noise due to the resulting shape of the frequency spectrum [26,27]. A primary source of these fluctuations is resting-state variations in T_2^* due to naturally occurring metabolic changes that are not specifically related to a task. These fluctuations have been used to investigate the "resting-state network" of neuronal connectivity in the brain [27]. They have been shown to be most prominent in gray matter [26], to peak at TE~T_2^* (since they rely upon the same mechanism as the BOLD effect) and to have much greater power than respiratory and cardiac fluctuations in BOLD-weighted images [25]. In the current study, these low frequency fluctuations in T_2^* manifest as fluctuations in the signal intensity of the raw tag and control ASL images. As the BOLD time series is formed by taking a surround average of the tag and control time series, these low frequency components are not attenuated in the BOLD time series [21]. In contrast, the perfusion time series is created by taking a surround subtraction of the raw data. As the surround subtraction operation is equivalent to demodulation followed by low pass filtering [21], low-frequency fluctuations in the raw data are shifted to high frequencies and then attenuated. As a result, low frequency fluctuations in the raw data are not a dominant noise source in the perfusion time series.

The temporal SNR values of the gray matter short-TE BOLD time series were not significantly different to the predicted values. In addition, the temporal SNR values of the white matter BOLD and short-TE BOLD time series were either not significantly different from (R=2) or significantly lower (R=3) than the predicted values. These findings are consistent with the minimal presence of physiological noise components (cardiac, respiratory and low-frequency

fluctuations) in both the short-TE gray matter BOLD data and the white matter data. The lower white matter values obtained for R=3 are consistent with a noise amplification that is slightly greater than unity, as was also observed in the image SNR results.

The mean F values measured within an active ROI were used to assess the functional sensitivity of the fMRI data. As expected, the BOLD data showed a reduction in the mean F value for the R=2 and R=3 data relative to the fully sampled data, and this was very consistent over a wide range of F thresholds. The corresponding SNR decrease was estimated using the square root of the mean F values; a comparison between these functional SNR decreases and the measured temporal SNR decreases found no significant difference. This suggests that the BOLD functional sensitivity can be predicted by the temporal SNR measurements.

The perfusion data also showed a reduction in the mean F for the undersampled relative to the fully sampled data. However, the reduction in the mean F was found to significantly decrease with an increase in the F threshold used to determine active voxels. This most likely reflects the fact that, for the perfusion data, we are operating in a relatively low SNR regimen. As the F threshold was increased, the relative fraction of voxels within the active ROI from the R=2 and R=3 reduction factors showed a steady decrease, resulting in a drop in the ROI-averaged F statistics at these reduction factors. This was not the case for the BOLD data where the relative contribution to the active ROI from the three reduction factors remained fairly stable (data not shown), reflecting the higher SNR of the BOLD data. The temporal SNR measurements cannot therefore be used to predict the functional sensitivity of the perfusion data, since the criteria for ROI have a significant influence.

Finally, it is worth noting that comparisons between fMRI studies employing parallel imaging techniques are not straightforward. The brain region being investigated (in particular whether artifacts related to long readouts are present), the acquisition technique (e.g., EPI vs. spiral), the parallel imaging method employed and the specific reconstruction parameters used must all be taken into account. The reconstruction parameters are particularly important; our group has recently shown [17] that the regularization term typically included in SENSE reconstruction [16] can have a significant effect on the expected SNR characteristics of the data. In essence, the inclusion of a regularization constraint is in some ways equivalent to introducing a level of smoothing that varies with reduction factor and can therefore directly impact SNR measures. In this study, we used a minimal regularization term with the aim of minimizing bias in our results. However, it is likely that most scanner manufacturer reconstruction software employs regularization to ensure convergence during iterative reconstruction methods, and full details must therefore be given in order that adequate comparisons can be made.

References

[1] Ra JB, Rim CY. Fast imaging using subencoding data sets from multiple detectors. Magn Reson Med 1993;30(1):142–5.

[2] Schmidt CF, Degonda N, Luechinger R, Henke K, Boesiger P. Sensitivity-encoded (SENSE) echo planar fMRI at 3T in the medial temporal lobe. Neuroimage 2005;25(2):625–41.

[3] Weiger M, Pruessmann KP, Osterbauer R, Bornert P, Boesiger P, Jezzard P. Sensitivity-encoded single-shot spiral imaging for reduced susceptibility artifacts in BOLD fMRI. Magn Reson Med 2002;48(5): 860–6.

[4] Preibisch C, Pilatus U, Bunke J, Hoogenraad F, Zanella F, Lanfermann H. Functional MRI using sensitivity-encoded echo planar imaging (SENSE-EPI). Neuroimage 2003;19(2 Pt 1):412–21.

[5] Luh WM, Wong EC, Bandettini PA, Ward BD, Hyde JS. Comparison of simultaneously measured perfusion and BOLD signal increases during brain activation with T(1)-based tissue identification. Magn Reson Med 2000;44(1):137–43.

[6] Duong TQ, Kim DS, Ugurbil K, Kim SG. Localized cerebral blood flow response at submillimeter columnar resolution. Proc Natl Acad Sci U S A 2001;98:10904–9.

[7] Davis TL, Kwong KK, Weisskoff RM, Rosen BR. Calibrated functional MRI: mapping the dynamics of oxidative metabolism. Proc Natl Acad Sci U S A 1998;95:1834–9.

[8] Wang J, Li L, Roc AC, Alsop DC, Tang K, Butler NS, et al. Reduced susceptibility effects in perfusion fMRI with single-shot spin-echo EPI acquisitions at 1.5 Tesla. Magn Reson Imaging 2004; 22(1):1–7.

[9] Wang Z, Wang J, Connick TJ, Wetmore GS, Detre JA. Continuous ASL (CASL) perfusion MRI with an array coil and parallel imaging at 3T. Magn Reson Med 2005;54(3):732–7.

[10] Pruessmann KP, Weiger M, Scheidegger MB, Boesiger P. SENSE: sensitivity encoding for fast MRI. Magn Reson Med 1999;42 (5):952–62.

[11] de Zwart JA, van Gelderen P, Kellman P, Duyn JH. Application of sensitivity-encoded echo-planar imaging for blood oxygen level-dependent functional brain imaging. Magn Reson Med 2002;48(6): 1011–20.

[12] Wong EC, Buxton RB, Frank LR. Implementation of quantitative perfusion imaging techniques for functional brain mapping using pulsed arterial spin labeling. NMR Biomed 1997;10:237–49.

[13] Wong EC, Buxton RB, Frank LR. Quantitative imaging of perfusion using a single subtraction (QUIPSS and QUIPSS II). Magn Reson Med 1998;39(5):702–8.

[14] Pruessmann KP, Weiger M, Bornert P, Boesiger P. Advances in sensitivity encoding with arbitrary k-space trajectories. Magn Reson Med 2001;46(4):638–51.

[15] Matej S, Fessler JA, Kazantsev IG. Iterative tomographic image reconstruction using Fourier-based forward and back-projectors. IEEE Trans Med Imaging 2004;23(4):401–12.

[16] Bydder M, Perthen JE, Du J. Optimization of sensitivity encoding with arbitrary k-space trajectories. Magn Reson Imaging 2007;25 (8):1123–9.

[17] Perthen JE, Bydder M, Restom K, Liu TT. SNR variation with regularization term for non-cartesian SENSE reconstruction. Book of abstracts: ISMRM; 2007. p. 290.

[18] Smith SM, Jenkinson M, Woolrich MW, et al. Advances in functional and structural MR image analysis and implementation as FSL. Neuroimage 2004;23(Suppl 1):S208–19.

[19] Cox RW. AFNI-software for analysis and visualization of functional magnetic resonance neuroimages. Comput Biomed Res 1996;29: 162–73.

[20] Glover GH, Lai S. Self-navigated spiral fMRI: interleaved versus single-shot. Magn Reson Med 1998;39(3):361–8.

[21] Liu TT, Wong EC. A signal processing model for arterial spin labeling functional MRI. Neuroimage 2005;24(1):207–15.

[22] Glover GH, Li TQ, Ress D. Image-based method for retrospective correction of physiological motion effects in fMRI: RETROICOR. Magn Reson Med 2000;44(1):162–7.
[23] Restom K, Behzadi Y, Liu TT. Physiological noise reduction for arterial spin labeling functional MRI. Neuroimage 2006;31(3):1104–15.
[24] Eggers H, Mazurkewitz P, Boesiger P. Noise amplification in parallel imaging. Book of abstracts: ISMRM Non-Cartesian MRI Workshop; 2007.
[25] Kruger G, Glover GH. Physiological noise in oxygenation-sensitive magnetic resonance imaging. Magn Reson Med 2001;46(4):631–7.
[26] Weisskoff RM, Baker J, Belliveau J, Davis TL, Kwong KK, Cohen MS, et al. Power spectrum analysis of functionally-weighted MR data: what's in the noise? Book of abstracts: SMRM; 1993. p. 7.
[27] Biswal B, Yetkin FZ, Haughton VM, Hyde JS. Functional connectivity in the motor cortex of resting human brain using echo planar MRI. Magn Reson Med 1995;34:537–41.